AFRL-AFOSR-VA-TR-2016-0094

Bayesian Computational Sensor Networks for Aircraft Structural Health Monitoring.

Thomas Henderson
UNIVERSITY OF UTAH SALT LAKE CITY

02/02/2016
Final Report

Air Force Research Laboratory
AF Office Of Scientific Research (AFOSR)/ RTA2
Arlington, Virginia 22203
Air Force Materiel Command

REPORT DOCUMENTATION PAGE

Form Approved
OMB No. 0704-0188

1. REPORT DATE *(DD-MM-YYYY)*	2. REPORT TYPE	3. DATES COVERED *(From - To)*
25-12-2016	Final Report	01-06-2013 -- 30-11-2015

4. TITLE AND SUBTITLE
Bayesian Computational Sensor Networks for Aircraft Structural Health Monitoring

5a. CONTRACT NUMBER
FA9550-12-1-0291

5b. GRANT NUMBER
FA9550-12-1-0291

5c. PROGRAM ELEMENT NUMBER
N/A

6. AUTHOR(S)
Thomas C. Henderson, V. John Mathews, Dan Adams

5d. PROJECT NUMBER
FA9550-12-1-0291

5e. TASK NUMBER
N/A

5f. WORK UNIT NUMBER
N/A

7. PERFORMING ORGANIZATION NAME(S) AND ADDRESS(ES)
University of Utah
Salt Lake City, UT 84112

8. PERFORMING ORGANIZATION REPORT NUMBER
N/A

9. SPONSORING/MONITORING AGENCY NAME(S) AND ADDRESS(ES)
Air Force Office of Scientific Research
875 N. Randolph St, Rom 3112
Arlington, VA 22203-1954

10. SPONSOR/MONITOR'S ACRONYM(S)
AFOSR

11. SPONSOR/MONITOR'S REPORT NUMBER(S)
N/A

12. DISTRIBUTION/AVAILABILITY STATEMENT
Unrestricted

13. SUPPLEMENTARY NOTES
N/A

14. ABSTRACT
Rigorous Bayesian Computational Sensor Networks are developed to quantify uncertainty in (1) model-based state estimates incorporating sensor data, (2) model parameters, (3) sensor node model parameter values (e.g., location, noise), and (4) input sources (e.g., cracks, holes). These decentralized methods have low computational complexity and perform Bayesian estimation in general distributed measurement systems (i.e., sensor networks). A model of the dynamic behavior and distribution of the underlying physical phenomenon is used to obtain a continuous form from the discrete time and space samples provided by a sensor network. This approach was applied to the aircraft structural health monitoring problem. Structural health monitoring (SHM) deals with evaluating structures for changes in their characteristics, predicting useful lifetime without maintenance, and recommending maintenance strategies to increase lifetime and reduce downtime. Current aircraft construction often involves fiber-reinforced laminated composite materials which offer certain advantages, but can suffer internal damage with little external evidence. We developed specific Bayesian computational models of SHM transducers (e.g., ultrasound) acting in both undamaged and damaged materials.

15. SUBJECT TERMS
Computational Sensor Networks; Bayesian Methods; Structural Health Monitoring

16. SECURITY CLASSIFICATION OF:			17. LIMITATION OF ABSTRACT	18. NUMBER OF PAGES	19a. NAME OF RESPONSIBLE PERSON
a. REPORT	b. ABSTRACT	c. THIS PAGE			Thomas C. Henderson
U	U	U	U U	16	19b. TELEPHONE NUMBER *(Include area code)* 801-581-3601

Final Performance Report: AFOSR

T.C. Henderson, V.J. Mathews, and D. Adams

Grant Number: FA9550-12-1-0291

AFOSR PI: Dr. Frederica Darema

25 January 2016

University of Utah, Salt lake City UT 84112

Executive Summary

The major goal of this work was to provide rigorous Bayesian Computational Sensor Networks to quantify uncertainty in (1) model-based state estimates incorporating sensor data, (2) model parameters (e.g., diffusion coefficients), (3) sensor node model parameter values (e.g., location, bias), and (4) input sources (e.g., cracks, holes). This was achieved in terms of extensions to our previously developed techniques. These decentralized methods have low computational complexity and perform Bayesian estimation in general distributed measurement systems (i.e., sensor networks). A model of the dynamic behavior and distribution of the underlying physical phenomenon is used to obtain a continuous form from the discrete time and space samples provided by a sensor network. This approach was applied to the aircraft structural health monitoring problem. Structural health monitoring (SHM) deals with evaluating structures for changes in their characteristics, predicting useful lifetime without maintenance, and recommending maintenance strategies to increase lifetime and reduce downtime. Current aircraft construction often involves fiber-reinforced laminated composite materials which offer certain advantages, but can suffer internal damage with little external evidence. We developed specific Bayesian computational models of SHM transducers (e.g., ultrasound) acting in both undamaged and damaged composite materials, and showed how to achieve simultaneous improved estimates of the physics model (e.g., diffusion and other coefficients), sensor node parameters (e.g., location, noise), input source parameters (e.g., crack or hole size and location). This framework has much broader application to many computational sensor networks, including medical, meteorological, general structural monitoring, and instrumented structures. This permits a mathematically precise characterization of the uncertainty in the state estimates of observed phenomena, as well as active control of sensor data acquisition to decrease that uncertainty.

The following goals were achieved:

1. A computational theory for selected sensor phenomena (heat, ultrasound) was developed. The heat problem was used as a first step in developing the computational methodology of BCSN, and ultrasound models were developed in terms of increasingly complex scenarios.
2. Model requirements on sensed data were specified for specific testing scenarios.
3. Distributed parameter system was extended to 2D case.
4. Macro feature phenomena exhibited in sensor data characterized.
5. Sensor network prototype developed.
6. Heat Plate experiments performed (Experiment 1).
7. Prior joint pdf's describing knowledge of model parameter distributions developed.
8. Robustness and stability of models under the various sources of perturbation (algorithmic, data, etc.) established.
9. Quantifiable validation processes to assess the appropriateness of the calibrated model for predictions of quantities of interest developed (e.g., damage existence, damage extent, model and sensor parameter values).
10. Piezoelectric active sensor network experimental results on metallic plates achieved (Experiments 2-4).

11. Methods for feedback driven active placement of sensors for variance reduction developed.
12. Input source pdf's from back-driven diagnosis scenario validation processes developed.
13. Critical aspects of the sensor network specifications required for iterative model parameter enhancement developed.
14. Solutions for inverse problems for localization, noise, etc. produced.
15. Results from physical validation experiments on all scenarios with composite plates described above achieved (Experiments 5-6).

The people who worked on this project include: Thomas C. Henderson, John Mathews, Jingru Zhou, Daimei Zhij, Ahmad Zoubi, Sabita Nahata, Dan Adams, Gwendolyn Knight, Kirill Rashkeev, Wenyi Wang, Anshul Joshi and Nishith Tirpankar. For more details on these results, see the resulting readily accessible publications [1,2,3,4,5,6,7,8,9,10,11,12,13,14,15,16,17,18].

An Overview of Results

Issues Related to Parameter Estimation in Model Accuracy Assessment

Model Accuracy Assessment (MAA) is an important part of the modern verification and validation process. This involves not only evaluation of a validation metric comparing experimental versus simulation system response quantities, but also the determination of the adequacy of the model for its intended use. We described some issues related to the use of parameter estimation on MAA in the study of heat flow in a 2D metal plate. We considered seven parameter estimation techniques, and showed that various factors such as length of sampling time, parameter estimation method, etc. impact the MAA. The ultimate goal is to improve MAA techniques in aircraft structural health care monitoring using Bayesian Computational Sensor Networks.

Model Accuracy Assessment in Reaction-Diffusion Pattern Formation in Wireless Sensor Networks

We demonstrated how to exploit reaction-diffusion (RD) patterns as part of the wireless sensor network (S-Net) high-level structure building toolkit; e.g., to support leader selection or to provide pathways through the network. In particular, we studied the formation of RD spot and stripe patterns in S-Nets for which no coordinate frame exists; i.e., the nets have only topological connectivity determined by the inter-node broadcast range. We further demonstrated how macro-features of the RD patterns can be used for Bayesian model accuracy assessment of the difference between a uniform grid layout of the nodes versus an irregular grid due to error in node placement.

SLAMBOT: Structural Health Monitoring Robot using Lamb Waves

We developed the combination of a mobile robot and a computational sensor network approach to perform structural health monitoring of structures. The robot is equipped with piezoelectric sensor actuators capable of sending and receiving ultrasound signals, and explores the surface of a structure to be monitored. A computational model of ultrasound propagation through the material is used to define two structural health monitoring methods: (1) a time reversal damage imaging (TRDI) process, and (2) a damage range sensor (DRS) (i.e., it provides the range to damaged areas in the structure). The damage in the structure is mapped using the DRS approach. The model is validated in an experimental setting.

Bayesian Computational Sensor Networks: Small-scale Structural Health Monitoring

The Bayesian Computational Sensor Network methodology is applied to small-scale structural health monitoring. A mobile robot, equipped with vision and ultrasound sensors, maps small-scale structures for damage (e.g., holes, cracks) by localizing itself and the damage in the map. The combination of vision and ultrasound reduces the uncertainty in damage localization. The data storage and analysis takes place exploiting cloud computing mechanisms, and there is also an on-line computational model calibration

component which returns information to the robot concerning updated on-board models as well as proposed sampling points. The approach is validated in a set of physical experiments.

Gaussian Processes for Multisensor Environmental Monitoring

Efficiently monitoring environmental conditions across large indoor spaces (such as warehouses, factories or data centers) is an important problem with many applications. Deployment of a sensor network across the space can provide very precise readings at discrete locations. However, construction of a continuous model from this discrete sensor data is a challenge. The challenge is made harder by economic and logistical constraints that may limit the number of sensor motes in the network. The required model, therefore, must be able to interpolate sparse data and give accurate predictions at unsensed locations, as well as provide some notion of the uncertainty on those predictions. We demonstrated a Gaussian process based model to answer both of these issues. We use Gaussian processes to model temperature and humidity distributions across an indoor space as functions of a 3-dimensional point. We studied the model selection process and showed that good results can be obtained, even with sparse sensor data. Deployment of a sensor network across an indoor lab provided real-world data that we used to construct an environmental model of the lab space. We refine the model obtained from the initial deployment by using the uncertainty estimates provided by the Gaussian process methodology to modify sensor distribution such that each sensor is most advantageously placed. We explored multiple sensor placement techniques and experimentally validated a near-optimal criterion.

The rest of this report clearly describes and illustrates the experimental equipment, set up, and procedures. We did not produce any archival datasets in this project, and all code development was of a prototype nature and no production level systems were produced.

Experimental Equipment, Setup and Procedures

A series of validation experiments were performed to support the development of the Bayesian Computational Sensor Networks (BCSNs). The initial experiments focused on heat conduction in aluminum plates and was used to validate the 2D BCSN simulations. However, all subsequent validation experiments focused on acoustic signal transmission in plate structures. Localized geometric complexities, including both holes and planar inclusions, were introduced into both aluminum and composite plates for use in detection, localization, and characterization. The objective of these experiments was to assess the capabilities of BCSNs in increasingly complex scenarios, and demonstrating their ability to detect and characterize carefully controlled anomalies introduced into the structure. Results from each type of experiment performed are summarized in the following sections.

Experiment 1: Steady state heat flow through a 2D thin isotropic plate

The first experiments focused on the temperature distribution in an aluminum plate subjected to conductive heat transfer. The end regions of the square plate were subjected to differing input temperatures and the temperature distribution in the central region was measured both using thermocouples at prescribed locations as well as with a thermographic (infrared) camera. Temperature distributions were compared between aluminum plates both with and without a central circular hole.

Figure 1 shows the experimental setup used. A FLIR T420 high performance IR camera produced a 320 x 240 pixel array, of which a 170 x170 subset sampled the aluminum plate. Figure 2 shows an example image with heat sources on the left and upper parts of the plate. To obtain smoother results for parameter estimation methods, the image was averaged down to a 17x17 grid.

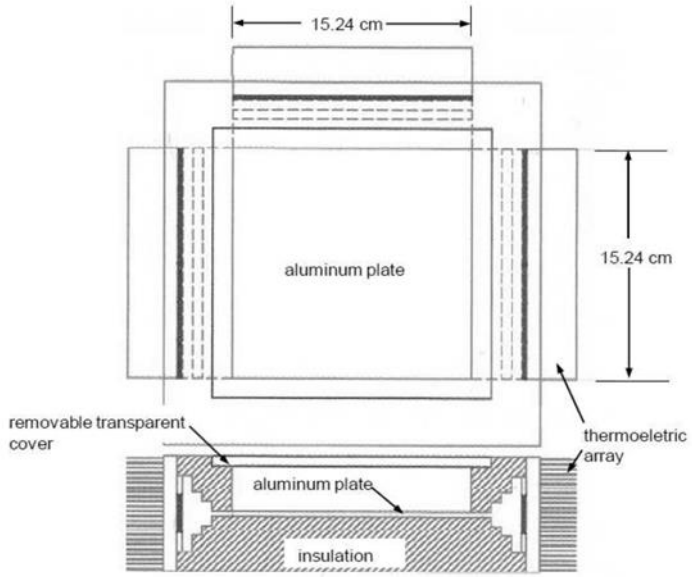

Figure 1. Experimental setup for 2-D conductive heat transfer experiments.

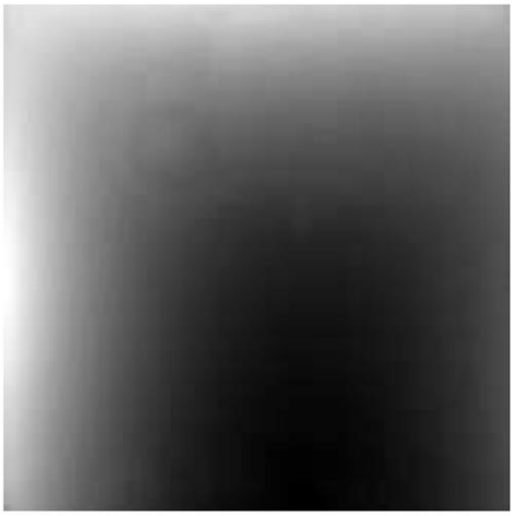

Figure 2. Example temperature distribution produced from IR camera during heat transfer experiment.

Experiment 2: Ultrasonic inspection of central inclusion in thin isotropic plate

The initial ultrasonic experiment was performed on the same type of aluminum plates (with and without centralized inclusions) that were used for heat flow experimentation. Additionally, carbon/epoxy

composite plates were used, as the use of composites were the final objective in this research project. For this set of experiments, the prescribed array of ultrasonic sensors were mounted onto the panels and the parameters of the model as well as uncertainty measures were calculated to assess the ability of the BCSN algorithms to accurately characterize the inclusions in the panel.

A series of 46 in. x 46 in. IM7/8552 carbon epoxy panels were fabricated. These composite panels were fabricated with a 16 ply quasi-isotropic stacking sequence, $[0_2/45_2/90_2/-45_2]_S$. A 1 in. diameter center hole was machined into one of the panels. Both Vallen VS900-M and Acellent sensors were utilized as both the actuator and the receiver sensor. The actuator and receiver sensors were located at several distances from each other (on opposite sides of the hole), ranging from 5 in. to 24 in. For these experiments, a 200 kHz 5 cycle tone burst source signal and a 2 MHz sampling rate was used.

Figure 3 shows the layout of the hole and sensors on the composite plate. The source signal was applied at A1, and the receiver was placed at R2 for investigating the no-hole condition. Similarly, the actuator at A2 and receiver at R2 were used for investigating the 1 in. diameter open hole condition. Signals were filtered in all ranges of 30-80 KHz, 30-300 KHz and 300-800 KHz. The best results were observed in the 30-300 KHz range for active sensing.

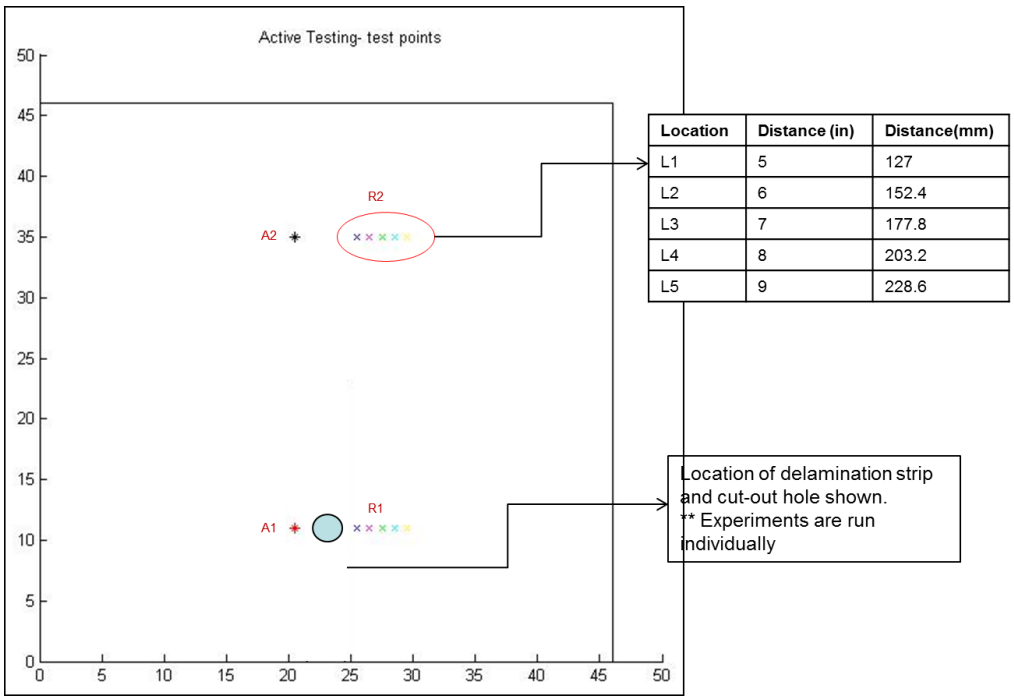

Location	Distance (in)	Distance(mm)
L1	5	127
L2	6	152.4
L3	7	177.8
L4	8	203.2
L5	9	228.6

Figure 3. Test panel layout showing hole and sensor locations.

Figure 4 shows time domain signals obtained for the cases of both a 1 in. diameter hole and the no-hole condition. In both cases, the receiver signal was placed at a distance of 24 in. from the source. Although a small difference in arrival time is observed, the estimated velocities have similar values due to the relatively large distance between the two sensors. While the initial portions of the received wave modes have clearly identifiable times of arrival, later arriving portions of the received wave modes become more complex due to complex interactions between multiple wave modes and reflections. Figure 5 shows differences in the first arrived wave group for the case of both a 1 in. diameter hole and the no-hole case.

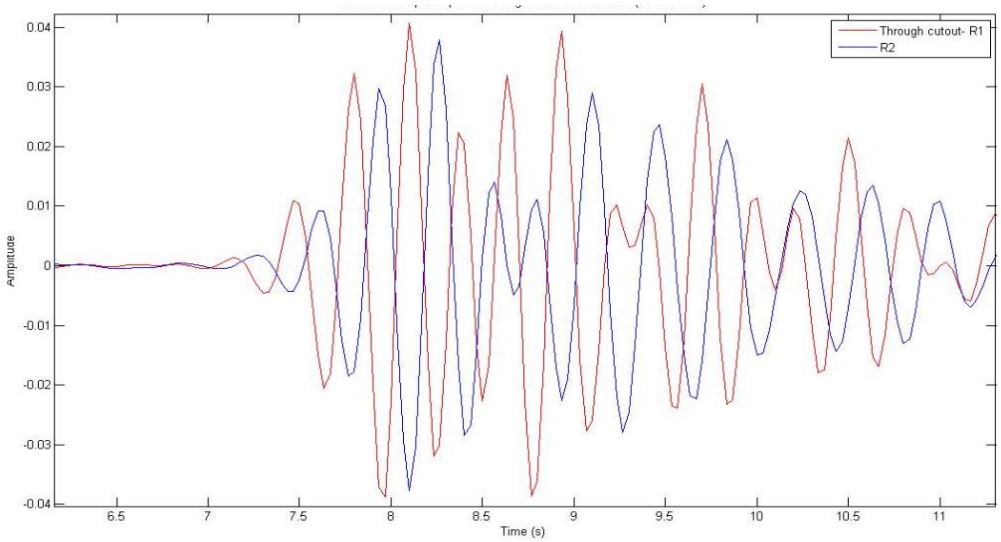

Figure 4. Time domain response for composite plate both with and without a 1 in. hole.

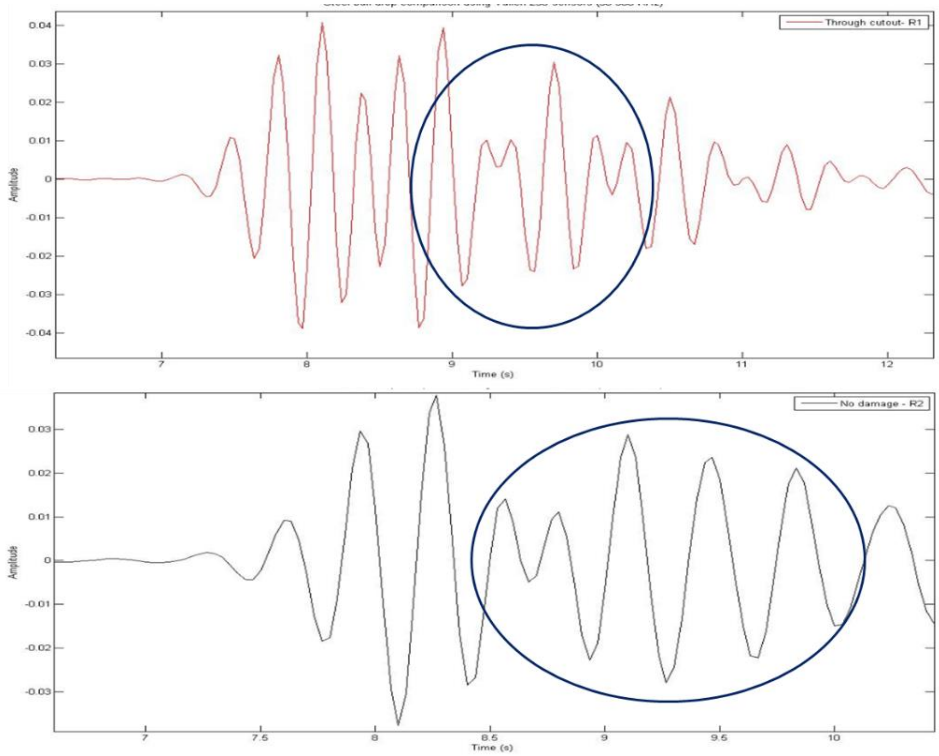

Figure 5. Magnified received signals showing differences in the first arrived wave group for the case of a 1 in. diameter hole (top) and the no-hole condition (bottom).

Experiment 3: Ultrasonic inspection of delaminated strip in bonded aluminum plate

The next round of ultrasonic experiments was performed on a two-layer, laminated aluminum plate structure with an unbonded strip, simulating an internal delamination. Two 46 in. x 46 in. aluminum plates

were bonded together using Cytec FM 300M film adhesive to form a two-layer isotropic laminate. In the central region of the bonded plate, a 3 in. wide unbonded strip was produced across one-half of the panel width by placing a thin Teflon film into the adhesive layer during manufacturing. This unbonded strip simulated an internal delamination for the idealized case of two isotropic (aluminum) material layers. Additionally, the other half of the bonded aluminum plate that did not contain a Teflon film strip was used as the control case (no disbond) for comparison testing. Vallen VS900-M sensors were utilized as both the actuator and the receiver sensor. The actuator and receiver sensors were located at several distances from each other (on opposite sides of the disbond), ranging from 5 in. to 24 in. For these experiments, a 200 kHz 5 cycle tone burst source signal and a 2 MHz sampling rate was used. Figure 6 shows the layout of the intentional disbond and the sensors on the aluminum plate. The source signal was applied at A1, and the receiver was placed at R1 for investigating the 3 in. wide internal disbond. Similarly, the actuator at A2 and receiver at R2 were used for investigating the no-disbond condition. Signals were filtered in the range of 30-300 KHz to achieve best results.

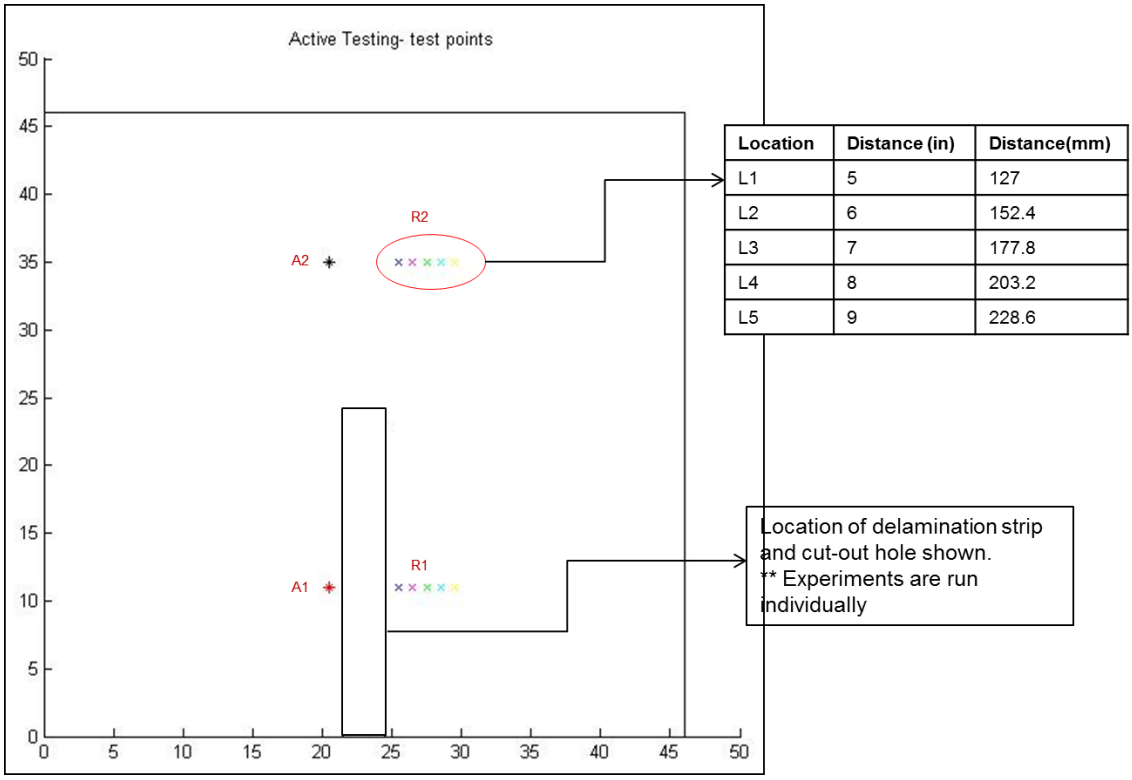

Location	Distance (in)	Distance(mm)
L1	5	127
L2	6	152.4
L3	7	177.8
L4	8	203.2
L5	9	228.6

Figure 6. Test panel layout showing intentional disbond and sensor locations.

Table 1 shows the changes in wave velocity due to the 3 in. wide disbond in the aluminum plate. Results suggest that a slightly higher velocity is produced by the disbond. However, the experimentally determined S_o wave mode velocity was determined to be roughly 7% less than the analytically estimated value obtained using the commercial code “Disperse” (5.4 mm/μs)

Table 1. Arrival Time and Estimated Velocity Effect of Disbond in Aluminum Plate

Type of Panel	Average Time of Arrival (μs)	Average S_o Mode Velocity (mm/μs)	Average Peak-to-Peak Difference Between Different Locations (μs)
No disbond (R2)	35.3	5.01	4.25
3 in. disbond (R1)	34.0	5.23	4.88

Experiment 4: Ultrasonic inspection of delaminated strip in a carbon/epoxy composite plate

Similar to the previous experiment, a through-width internal delamination was fabricated into a laminated carbon/epoxy composite plate. A 46 in. x 46 in. IM7/8552 carbon/epoxy panel was fabricated using the same 16 ply quasi-isotropic stacking sequence, $[0_2/45_2/90_2/-45_2]_s$ investigated previously. In the central region of the laminate, a 3 in. wide unbonded strip was produced across one-half of the panel width by placing a thin Teflon film into the carbon/epoxy laminate during layup as shown in Figure 7. The other half of the composite panel that did not contain a Teflon film strip was used as the control case (no delamination) for comparison testing. Vallen VS900-M sensors were utilized as both the actuator and the receiver sensor. The actuator and receiver sensors were located on opposite sides of the delamination in the same arrangement as used for the aluminum panel (Experiment 3) and shown in Figure 6. A 200 kHz, 5 cycle tone burst source signal and a 2 MHz sampling rate was used.

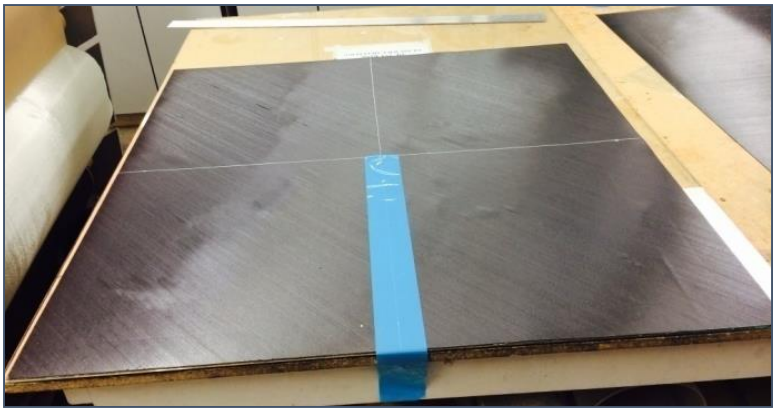

Figure 7. Teflon layer insertion for creating artificial delamination within carbon/epoxy composite panel.

Table 2 shows the changes in wave velocity due to the 3 in. wide disbond in the carbon/epoxy composite plate. Similar to the case for the aluminum plate, experimental results suggest that a slightly higher velocity was produced by the embedded delamination. Additionally, the experimentally determined S_o wave mode velocity was determined to be roughly 12% less than the analytically estimated value obtained using the commercial code “Disperse” (6.23 mm/μs)

Table 2. Arrival Time and Estimated Velocity Effect of Disbond in Composite Plate

Type of Panel	**Average Time of Arrival (μs)**	**Average So mode velocity (mm/μs)**	**Average peak-to-peak difference (μs)**
No disbond	44.0	5.45	4.1
3 in. disbond	40.4	6.14	4.0

Experiment 5: Ultrasonic inspection of simulated impact damage in composite plate:

To investigate a more complex form of damage similar to that produced by a blunt impact of a composite plate, stacked delaminations were fabricated into the central region of a carbon/epoxy composite plate. To different delamination formations were fabricated using Teflon inserts, placed at different through-the-thickness layer interface locations in the composite layup. The first delamination formation fabricated was a 1.5 in. wide delamination strip that was positioned at the mid-thickness of the quasi-isotropic $[0/45/90\text{-}45]_s$ composite panel. The second delamination formation fabricated was a stacked delamination consisting of a 1.5 in. wide delamination placed 25% of the distance through the composite laminate and a second 1.5 in. wide delamination placed mid-thickness. As was the case in the previous experiment, IM7/8552 carbon/epoxy was used to fabricate the panels. Figure 8 shows a cross section of the two panels, illustrating the region with the embedded delaminations.

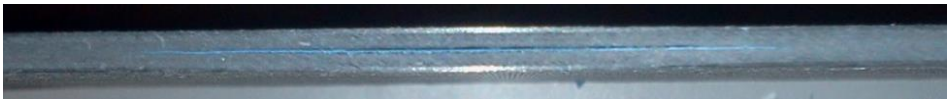

a) Single delamination

b) Stacked delamination

Figure 8. Cross section with embedded delaminations in carbon/epoxy composite panels.

Testing was performed using both Vallen VS900-M and Vallen VS900RIC sensors. The actuator and receiver sensors were located on opposite sides of the delamination in the same arrangement as used for the previous experiments (Experiments 3 and 4). A 150 kHz, 5 cycle tone burst source signal and a 2 MHz sampling rate was used. Data was acquired for a total of 1000 µs (1 ms) for each test. Fast Furrier Transform (FFT) analysis was performed to investigate the frequency response up to 1 MHz. For each condition, a total of 10 replicate tests were conducted to investigate repeatability and consistency. Figure 9 shows the test conditions and sensor positions used.

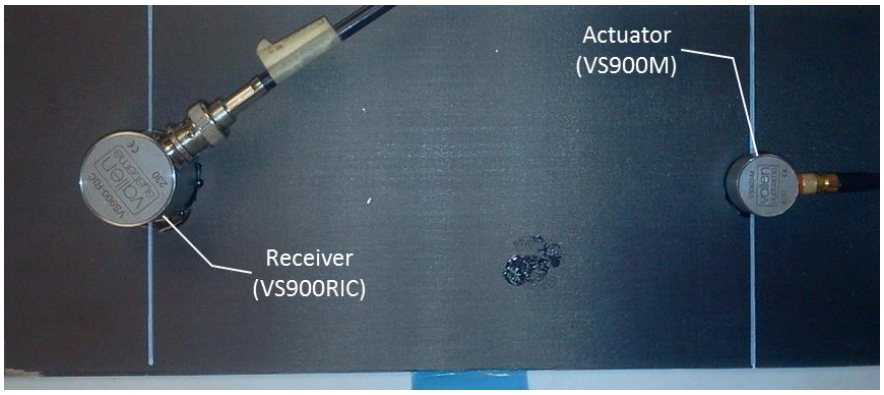

Figure 9. Experimental setup used for investigating stacked delaminations.

Figure 10 shows both the time domain and frequency domain signals obtained for the cases of the single 1.5 in. delamination in the composite plate. Similarly, Figure 11 shows the time and frequency domain signals for the two stacked delaminations. A comparison of the two sets of results shows that the stacked

delaminations led to a decrease in signal amplitude at the receiving sensor than the single delamination condition. This result is believed to be a result of the energy dissipation produced by the increasing number of internal surfaces within the laminate. In general, the overall envelopes of the received waves show differences due to wave distortions. While the FFT results from the single delamination display a focused peak amplitude at 150 kHz, the stacked delamination case shows scattered peaks in the frequency domain, both above and below this 150 kHz frequency.

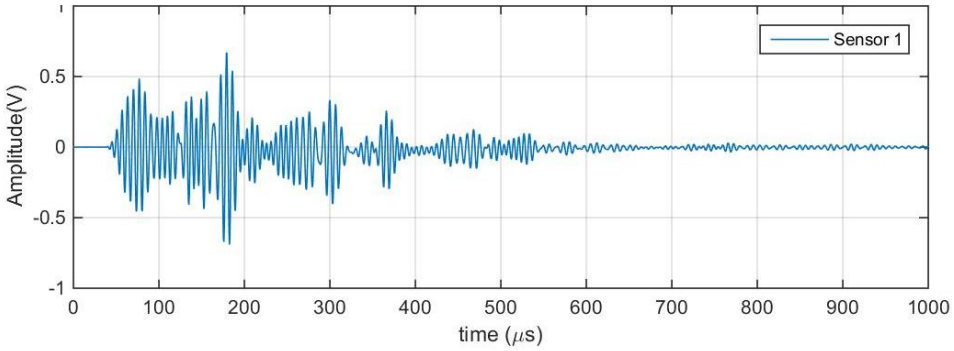

a) Signal response in time domain.

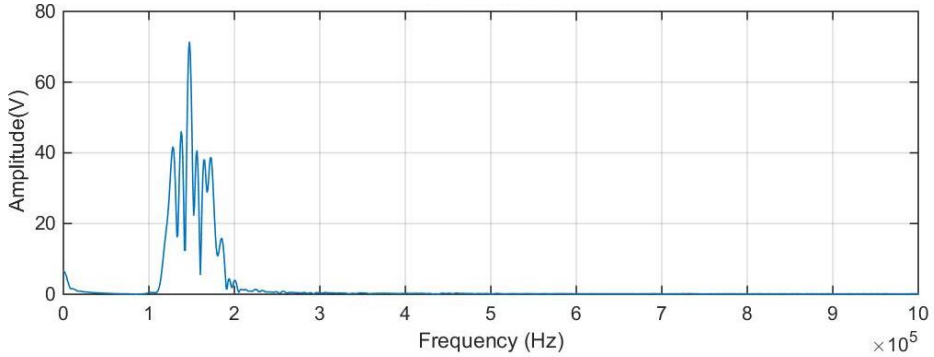

a) Signal response in frequency domain.

Figure 10. Signal responses for composite plate with embedded 1.5 in. delamination.

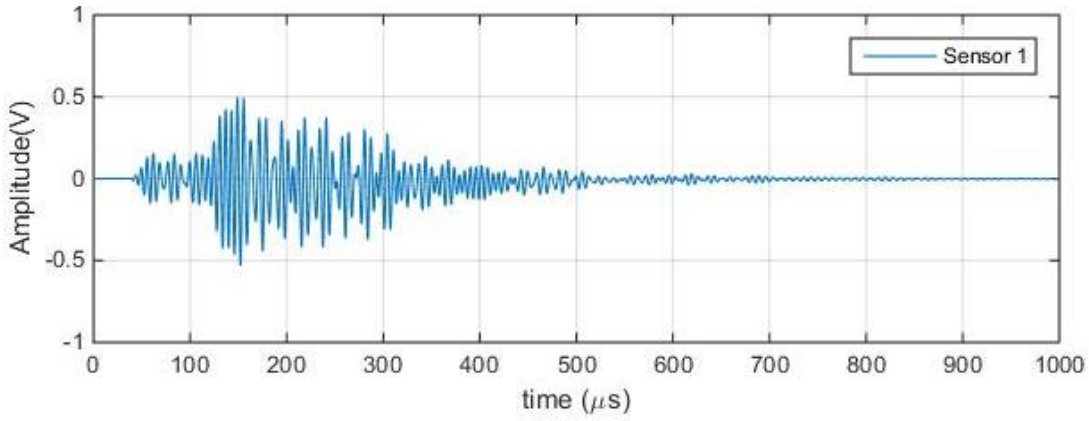

a) Signal response in time domain.

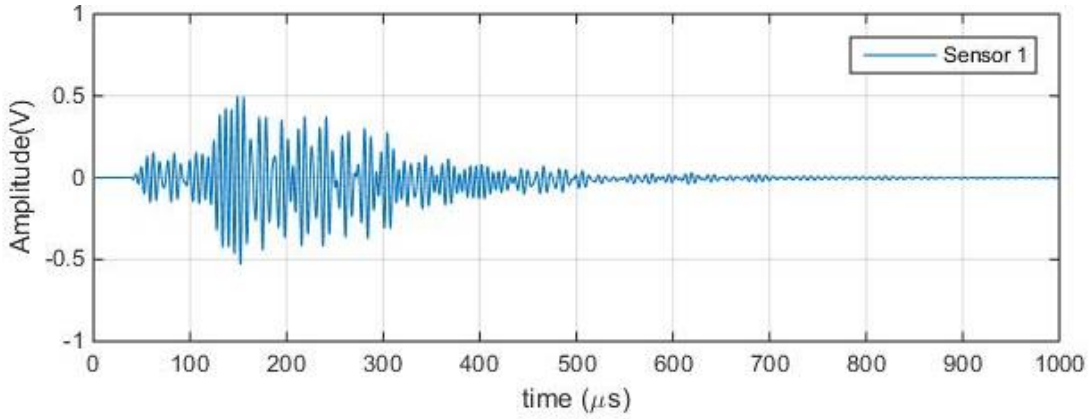

a) Signal response in frequency domain.

Figure 11. Signal responses for composite plate with two stacked 1.5 in. delaminations.

Experiment 6: Ultrasonic inspection of low-velocity blunt impact damage in composite plates

As a final validation experiment, a series of carbon/epoxy composite plates were subjected to actual impact events using a blunt-nose impactor. The first task associated with these experiments was determining the impact energies and support conditions to produce barely visible, delamination-dominated impact damage. Following these initial trial impacts, follow-on impact tests were performed with AE sensors attached to the specimens to record and investigate the characteristics of the received signals.

Similar to the previous experiments a series of 16 ply quasi-isotropic carbon/epoxy composite plates were fabricated. The plates were cut to 18 in. x 20 in. sections for impact testing. Impacting was performed using a 1 in. diameter hemispherical impactor and an impact mass of 10.9 lbs as shown in Figure 12. Two sensor types were used at the centerline of the panel: Digital Wave B-1025T and Vallen VS900-M. Each sensor was located a distance of 5 in. from the impact location. In addition to the received sensor signals, an impact force versus time response was recorded for each impact. Following impacting, each impact specimen was ultrasonically C-scanned for establishing the delamination damage produced. Table 3 shows the impact conditions used for the experiments. Two drop heights were used: 8 in. and 16 in. Figure 13 shows the ultrasonic C-scan results from both impact conditions, displaying the size of the damage region near the top surface, in the upper half of the panel thickness, and throughout the entire thickness.

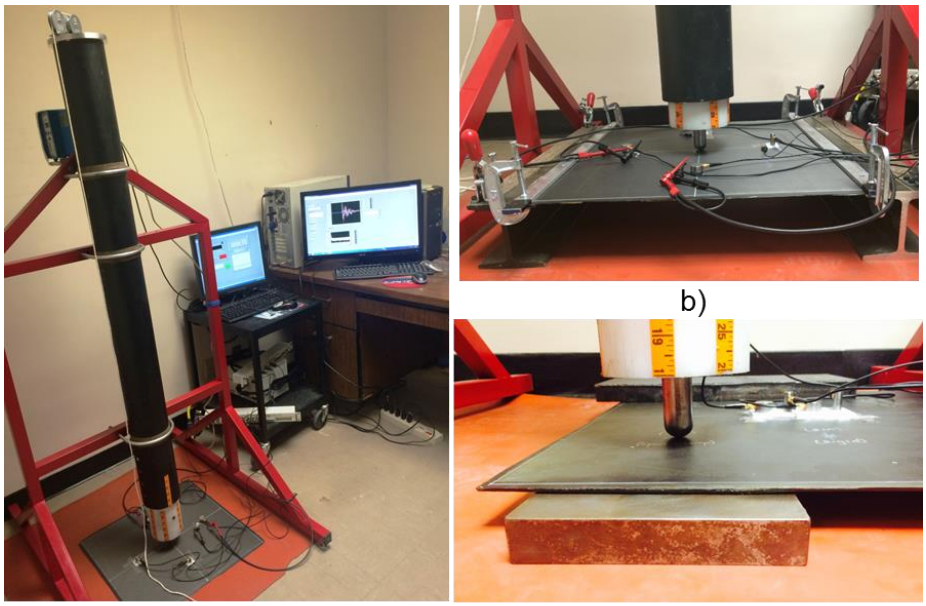

Figure 12. Experimental set-up used for impact testing: a) Impact tower; b) Edge clamped boundary; c) Simply supported boundary conditions.

Table 3. Impact Test Parameters Used With Simply Supported Conditions

Boundary conditions	Drop Height (in.)	Potential Energy (ft-lbf)	Impact Energy (ft-lbs)	Peak Load (lbf)	Impact Velocity (in./s)	Displacement (in.)
Simply Supported, 6 in. x 3 in. opening	8	9.5	8.23	808	79	0.35
	16	18.9	17.2	1,126	111	0.41

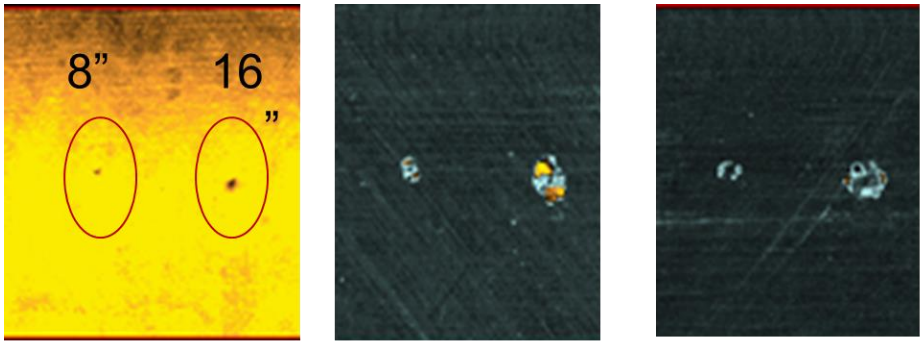

Figure 13. Ultrasonic C-scan results showing damage areas for the 8 in. and 16 in. impact heights.

Figures 14 and 15 show received sensor signals corresponding to three different filter ranges for both the 8 in. and 16 in. drop height impacts. Using initial testing and analysis in both the time and frequency domains, three frequency ranges were identified that appeared to contain elastic acoustic emissions as well as delamination-dominated and fiber-dominated damage. The three frequency regions identified were 10 - 100 kHz, 100 - 250 kHz, and 250 - 500 kHz. In Figures 14 and 15, the red lines represent raw signals measured by sensors and blue lines represent the filtered signals according to each filtering range. Results obtained in these experiments suggest that damage creation is best observed in the 100 - 500 kHz filtered range.

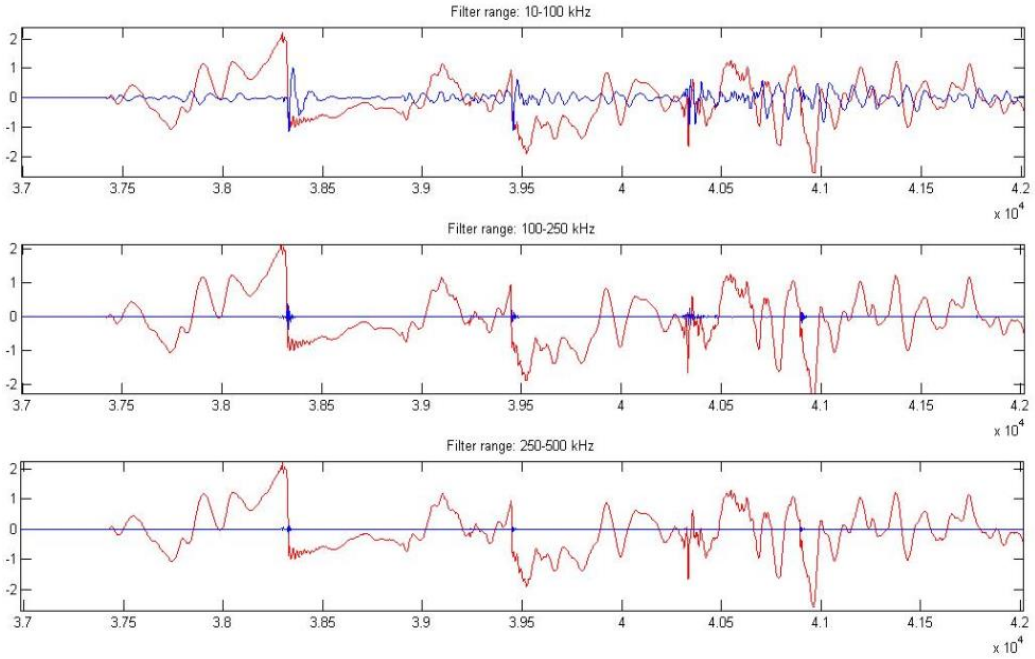

Figure 14. Received sensor signals from 8 in. drop impact.

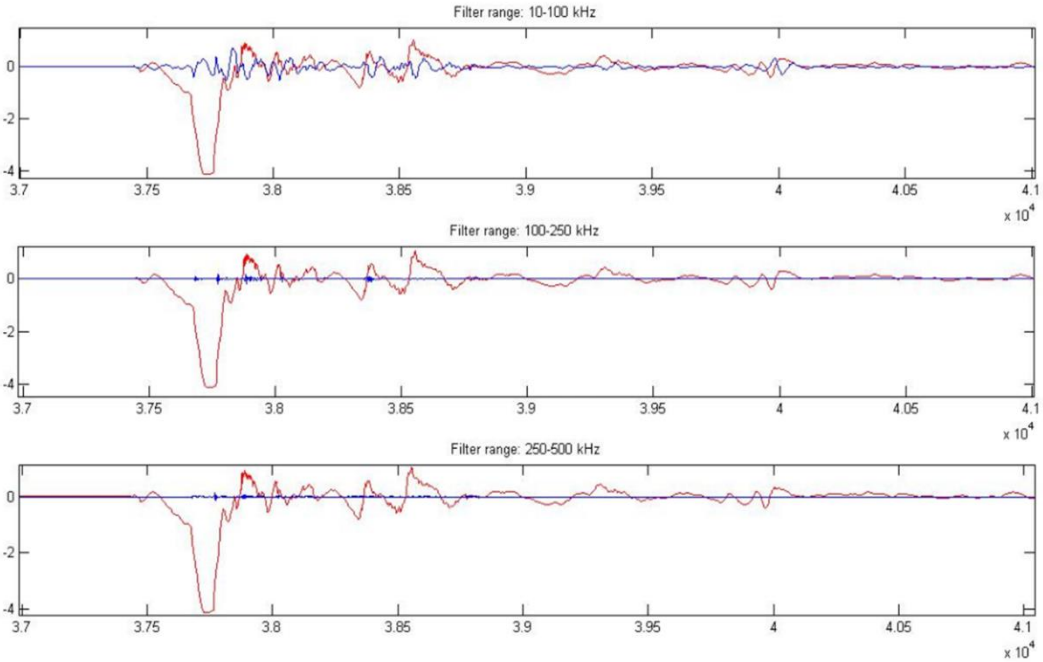

Figure 15. Received sensor signals from 16 in. drop impact.

References

[1] ``Multisensor Methods to Estimate Thermal Diffusivity,'' Thomas C. Henderson, Gwen Knight and Edward Grant, IEEE Conference on Multisensor Fusion and Integration, Hamburg, Germany, September 2012.

[2] ``Reaction-Diffusion Computation in Wireless Sensor Networks,'' Thomas C. Henderson, Kyle Luthy and Edward Grant, Workshop on Unconventional Approaches to Robotics, Automation and Control Inspired by Nature, IEEE International Conference on Robotics and Automation, Karlsruhe, Germany, pp. 13-15, 6-10 May, 2013.

[3] ``Issues Related to Parameter Estimation in Model Accuracy Assessment,'' Thomas C. Henderson, and Narong Boonsirisumpun, Workshop on Dynamic Data Driven Analysis Systems, Barcelona, Spain, 5-7 June, 2013.

[4] ``Model Accuracy Assessment in Reaction-Diffusion Pattern Formation in Wireless Sensor Networks,'' Thomas C. Henderson, Anshul Joshi, Kirril Rashkeev, Narong Boonsirisumpun, Kyle Luthy and Edward Grant, University of Utah Technical Report, UUCS-13-003, Salt Lake City, UT, May 2013.

[5] ``Robot Cognition using Bayesian Symmetry Networks,'' Anshul Joshi, Thomas C. Henderson, and Wenyi Wang , Proceedings of the International conference on Agents and Artificial Intelligence, Angers, France, 6-8 March 2014.

[6] ``Bayesian Methods for Aircraft Structural Health Monitoring,'' T.C. Henderson, V.J. Mathews, D.O. Adams, W. Wang, S. Nahata, N. Boonsirisumpun, A. Joshi and E. Grant , in Dynamic Data Driven Application Systems, Ed. F. Darema, Springer, to appear.

[7] ``Model Accuracy Assessment in Reaction-Diffusion Pattern Formation in Wireless Sensor Networks,'' Thomas C. Henderson, Anshul Joshi, Kirril Rasjkeev, Narong Boonsirisumpun, Kyle Luthy, Edward Grant, International Journal of Unconventional Computing, Vol. 10, No. 4, pp. 317-338, 2014.

[8] ``SLAMBOT: Structural Health Monitoring using Lamb Waves,'' Wenyi Wang, Thomas C. Henderson, Anshul Joshi and Edward Grant, IEEE Conference on Multisensor Fusion and Integration for Intelligent Systems, Beijing, Sept. 28-30, 2014.

[9] ``SLAMBOT: Structural Health Monitoring using Lamb Waves,'' Wenyi Wang, Thomas C. Henderson, Anshul Joshi and Edward Grant, IEEE Conference on Multisensor Fusion and Integration for Intelligent Systems, Beijing, Sept. 28-30, 2014.

[10] ``Bayesian Computational Sensor Networks: Small-scale Structural Health Monitoring,'' Wenyi Wang, Anshul Joshi, Nishith Tirpankar, Philip Erickson, Michael Cline, Palani Thagaraj, and Thomas C. Henderson, International Conference on Computational Science, Reykavik, Iceland, June 1-3, 2015.

[11] ``Gaussian Processes for Multi-Sensor Environment Modeling,'' Philip Erickson, Michael Cline, Nishith Tirpankar and Thomas C. Henderson, Proceedings IEEE Conference on Multisensor Fusion and Integration for Intelligent Systems, San Diego, CA, Sept 14-16, 2015.

[12] ``Impact Location Estimation in Anisotropic Structures,'' J. Zhou and V. J. Mathews, Proceedings of QNDE 2014, Boise, Idaho, July 21-25, 2014.

[13] ``Damage Mapping in Structural Health Monitoring Using a Multi-Grid Architecture,'' V. J. Mathews, Proceedings of QNDE 2014, Boise, Idaho, July 21-25, 2014.

[14] ``A Comparative Evaluation of Piezoelectric Sensors for Acoustic Emission-Based Impact Location Estimation and Damage Classification in Composite Structures,'' B. Uprety, S. Kim, D. O. Adams and V. J. Mathews, Proceedings of QNDE 2014, Boise, Idaho, July 21-25, 2014.

[15] ``Numerical Simulation and Experimental Validation of Lamb Wave Propagation Behavior in Composite Plates,'' S. Kim, B. Uprety, D. O. Adams and V. J. Mathews, Proceedings of QNDE 2014, Boise, Idaho, July 21-25, 2014.

[16] ``Lamb wave mode decomposition using the cross-Wigner-Ville distribution,'' A. B. Zoubi, V J. Mathews, J. B. Harley and D. O. Adams, Proceedings of the International Workshop on Structural Health Monitoring, Sep. 1-3, Stanford, CA, 2015.

[17] ``Acoustic Emission-Based Impact Location Estimation for Composite Structures,'' A. B. Zoubi, V J. Mathews, and D. O. Adams, Proceedings of the International Workshop on Structural Health Monitoring, Sep. 1-3, Stanford, CA, 2015.

[18] ``Acoustic Emission Based Damage Characterization in Composite Plates Using Low-Velocity Impact Testing,'' S. Kim, B. Uprety, D. O. Adams, V J. Mathews and J. B. Harley, Proceedings of the International Workshop on Structural Health Monitoring, Sep. 1-3, Stanford, CA, 2015.